Finite Element Method Based Estimation of Critical Current Density of NbTi

Finite Element Method Based Estimation of Critical Current Density of NbTi

Joonas Vesa[1], Valtteri Lahtinen[1,2], Paavo Rasilo[1]
[1]Unit of Electrical Engineering, Tampere University, Tampere, 33720 Finland
[2] QCD Labs, QTF Centre of Excellence, Department of Applied Physics,
Aalto University, FI-00076 Aalto, Finland

The purpose of this paper is to estimate the magnetic field dependent critical current density scaling relation of NbTi used in a superconducting wire. The estimation problem is set using a finite element method based forward model solving the critical current of a wire in external magnetic fields. A sensitivity analysis is carried out to reveal the uncertainties in the process. It is shown that the methods provide accurate predictions of critical currents in a wire, but there are uncertainties related to the zero-field critical current density of the material.

***Index Terms*—Estimation, Inverse problem, Material identification, NbTi, Scaling relation, Superconductor.**

I. Introduction

TYPE II superconductive materials accept simultaneous presence of magnetic field and supercurrents in the material. These fields are not independent of each other but the critical current density scales with respect to magnetic field and other quantities, such as temperature and strain.

It has been established in the literature that self-field effects of superconducting cables affect the critical current of the cable, especially if externally applied magnetic field is low [1]. This raises some questions about the traditional definition of critical current density, where the critical current density is defined as the critical current of a cable divided by the cross sectional area of the superconductive material. The problem is well-known, and proposals for taking the self-fields into account have been reported [2].

This paper introduces and trials a finite element (FE) method based estimation scheme of critical current density scaling relations. It should be noted that computational estimations of critical current density relations have been reported before. Rostila *et al.* used Biot-Savart type volume integration methods and Nelder-Mead algorithm to fit a modified Kim model to represent the critical current density [3].

We also note the work of Grilli *et al.* for implementing similar ideas in commercial FE solvers with a brute-force inverse approach [4]. It was pointed out that the existing methods are often based on Nelder-Mead optimization, brute-force or avoiding explicit optimizations. Zermeño *et al.* estimated an unparametrized form of critical current density using a gradient-free hill climbing algorithm [5]. Both of these papers contain well-written literature reviews of inverse estimations of critical current density relations [4],[5].

This paper uses a trust region method applied to an optimization problem providing fast convergence. In this context, we do not consider angular dependencies of the critical current density.

Manuscript received December 20, 2019; revised April 26, 2020. Corresponding author: J. Vesa (https://tutcris.tut.fi/portal/en/persons/joonas-vesa(c7791107-71f3-413e-a85e-f8b4b7424509).html). V. Lahtinen is currently with Aalto University. The contribution by V. Lahtinen for this paper was done partially as a post-doctoral researcher at Tampere University.

II. Problem

Spencer *et al.* measured the critical current of a 180-filament NbTi wire in various externally applied magnetic fields and various temperatures [6]. A schematic figure of the wire is presented in Fig. 1. This figure is much like the cross sectional image of the wire Spencer *et al.* reported. The diameter of the wire was reported to be $0.81\ \mathrm{mm}$ and the filaments, surrounded by copper, were $35\ \mu\mathrm{m}$ thick.

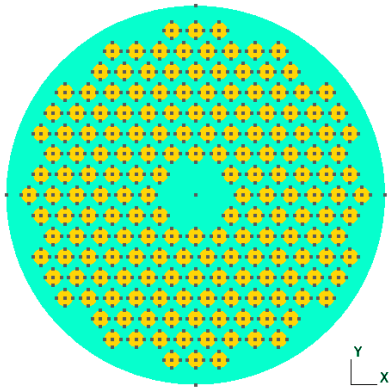

Fig. 1. A schematic image of a cross section of an NbTi superconductor. The wire diameter is $0.81\ \mathrm{mm}$ and the filaments are $35\ \mu\mathrm{m}$ thick.

It was reported that the wire carries critical currents, dependent on externally applied magnetic field, as depicted in Fig. 2 [6]. The problem is to find a critical current density scaling relation $j_\mathrm{c}(h)$ for the filaments such that a FE problem defined on the geometry of Fig. 1 provides a curve imitating the measurements well.

III. Computational model

Before inverse estimation may be performed, the forward model should be discussed. The key ideas of the forward

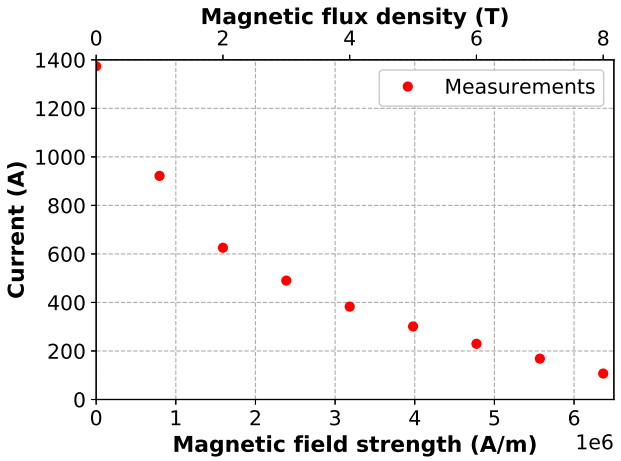

Fig. 2. Critical current measurements in 4.2 K according to Spencer *et al.* [6].

model can be found in the literature, for instance in the works of Zermeño *et al.* [7].

As a shortcut, we do not consider twisting of the wire. Simple translational symmetry is assumed for the conductor. Furthermore, the filaments are assumed to be fully coupled. Possible extensions to the model are discussed later in Section VI.

A. Field problem

We assume that in the cross sections of the wire in critical state, the current density j is equal to the critical current density $j_{\mathrm{c}}(h)$ in the superconductive materials. A formulation of a magnetic vector potential equation could be formed around the Ampère law $\mathrm{curl}(h) = j_{\mathrm{c}}(h)$ in the superconductive materials and $\mathrm{curl}(h) = 0$ elsewhere. The critical current is then obtained by integrating $j_{\mathrm{c}}(h)$ over the conductor cross section. In this paper, we write the problem in terms of a co-potential formulation for h instead of a potential formulation for b. In the end, the concrete computations are the same, except for a scaling of the potential by the vacuum permeability μ_0. The machinery of differential forms is used [8]. This formalism is an accepted formalism in the field of computational electromagnetics [9] and has been utilized in the field of applied superconductivity [10], [11], [12].

Consider the geometry in Fig. 1. Consider a domain Ω consisting of the superconductive regions Ω_{s}, copper Ω_{Cu}, and air Ω_{a}, whose boundary is relatively far from the boundary of the wire. Assuming an externally applied field h_{ext}, we write the unknown h as $h = h_{\mathrm{ext}} + \star \mathrm{d}\varphi$. Furthermore, it is assumed that $\mathrm{d}h_{\mathrm{ext}} = 0$. The equation for φ reads as

$$\mathrm{d} \star \mathrm{d}\varphi = \begin{cases} j_{\mathrm{c}}(\|h\|)\mathrm{Vol}, & \text{on } \Omega_{\mathrm{s}}, \\ \sigma_{\mathrm{c}} e_{\mathrm{c}}, & \text{on } \Omega_{\mathrm{Cu}}, \\ 0, & \text{on } \Omega_{\mathrm{a}}, \end{cases} \tag{1}$$

where Vol is the volume form, σ_{c} is the conductivity operator of copper and e_{c} is a characteristic electric field of the superconductor, and most importantly, j_{c} is the critical current density scaling relation of the superconductive material. We set $\varphi = 0$ on $\partial\Omega$. Equation (1) is discretized using the Galerkin method with nodal scalar basis.

The forward model I_{c} accepts a scalar h_{sc} as an input, sets $h_{\mathrm{ext}} = h_{\mathrm{sc}} dy$ and solves φ from the discretized version of (1). Then the current density

$$j = \begin{cases} j_{\mathrm{c}}(h), & \text{on } \Omega_{\mathrm{s}}, \\ \sigma_{\mathrm{c}} e_{\mathrm{c}}, & \text{on } \Omega_{\mathrm{Cu}}, \end{cases} \tag{2}$$

is computed and integrated over $\Omega_{\mathrm{s}} \cup \Omega_{\mathrm{Cu}}$ to obtain the critical current $I_{\mathrm{c}}(h_{\mathrm{sc}})$ as an output. In the end, I_{c} is just a computational model for the measurements depicted in Fig. 2. In order to obtain any sort of agreement between I_{c} and the measurements, the critical current density j_{c} is parametrized and the parameters estimated in a systematic manner.

B. Parametrization of the scaling relation

To construct a meaningful parametrized scaling relation, we define several approximating functions $f_1, ..., f_n$ and express j_{c} as a linear combination of the functions. We used a similar approach to express the magnetization of soft magnetic composite materials [13].

Bottura *et al.* have used scaling relations of the form $I_{\mathrm{c}} \sim b^{\alpha}(1-b)^{\beta}$, where b is reduced magnetic flux density and α and β are fitting parameters [14], [15]. We set

$$f_i(\|h\|) = \alpha_i \left(1 - \frac{\|h\|}{h_{\mathrm{c2}}}\right)^{q_i},$$

where α_i and q_i are fitting parameters and h_{c2} is the upper critical field of the material. The numerical value of $h_{\mathrm{c2}} \approx 11.4332\ \mathrm{T}/\mu_0$ in 4.2 K was extrapolated from the upper critical field values reported by Spencer *et al.* [6]. We choose four basis functions with

$$q_1 = 1, \quad q_2 = 4, \quad q_3 = 16, \quad q_4 = 64$$

and we set

$$j_{\mathrm{c}}(\|h\|, \alpha) = \sum_{i=1}^{4} \alpha_i \left(1 - \frac{\|h\|}{h_{\mathrm{c2}}}\right)^{q_i}, \tag{3}$$

which gives a parameterized family of scaling relations whose parameters $\alpha = [\alpha_1, \alpha_2, \alpha_3, \alpha_4]$ should be estimated.

C. Estimation problem

We denote the measured values of the critical curve in Fig. 2 as $(h_{\mathrm{meas},i}, I_{\mathrm{c,meas},i})$, with $i = 1, ..., 9$. Using the parameterized critical current density scaling relation (3) in the FE discretized version of (1), the forward model $I_{\mathrm{c}}(h_{\mathrm{sc}}, \alpha)$ returns the integral of (2) over the cross section of the wire in Fig. 1. We seek for parameters α that minimize the error function

$$e(\alpha) := \left(\sum_{i=1}^{9} \left[I_{\mathrm{c,meas},i} - I_{\mathrm{c}}(h_{\mathrm{meas},i}, \alpha) \right]^2 \right)^{1/2}. \tag{4}$$

The minimization was carried out using the Trust Region Reflective algorithm implemented in the Scipy optimization package [16]. The α-values obtained from the minimization problem are given by

$$\alpha \approx [2.49, 3.60, 3.04, 29.2] \cdot 10^9 \mathrm{A/m}^2. \tag{5}$$

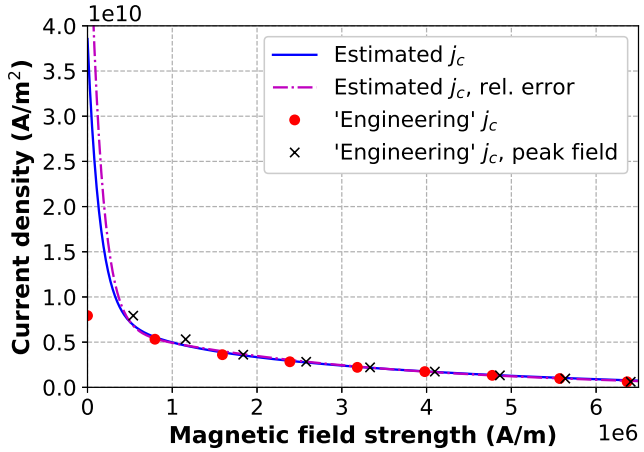

(a) Large scale plot

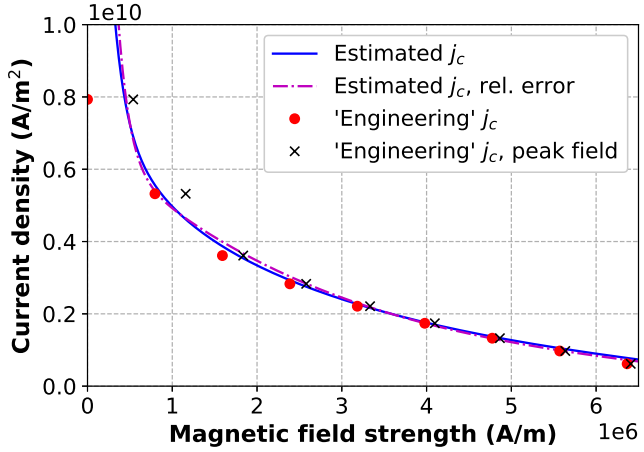

(b) Small scale plot

Fig. 3. Estimated critical current densities in 4.2 K. The 'engineering' current density is computed by dividing the critical currents of the wire by the cross sectional area of the superconductive filaments.

The estimated j_c is depicted in Fig. 3a and b as 'Estimated j_c'. In the figures, there is also an 'Engineering' j_c, which is defined just by dividing the measured critical currents by the cross sectional area of the superconducting filaments. We see that the greatest differences between the 'engineering' j_c and the estimated j_c can be found in the region of low external magnetic fields.

Furthermore, in Fig. 3, we see an additional critical current density, called 'Estimated j_c, rel. error'. This curve was obtained using the error function

$$e_2(\alpha) := \left(\sum_{i=1}^{9} \left[\frac{I_{\mathrm{c,meas},i} - I_c(h_{\mathrm{meas},i}, \alpha)}{I_{\mathrm{c,meas},i}} \right]^2 \right)^{1/2} \tag{6}$$

instead of (4). Since the discrepancy between 'Estimated j_c, rel. error' and 'Estimated j_c' in Fig. 3 is small at least above 500 kA/m, we conclude that the estimation of the critical current density is not overly dependent on the chosen error function. The sensitivity of the zero-field critical current density is discussed further in Section V.

In Fig. 3, there are also crosses marking an 'Engineering j_c, peak field'. These datapoints are just the engineering critical current density points plotted against peak field corrected magnetic fields proposed by Garber *et al.* [2]. The peak field correction is given by

$$H_{\mathrm{p}} = H_{\mathrm{ext}} + \frac{I}{\pi D}, \tag{7}$$

where H_{ext} is the magnitude of the externally applied field, I is the net current through the wire and D is the wire diameter. It seems that the peak field corrected engineering current densities agree better with the estimated results than without the correction. In this case, the peak field corrected results are not defined below ∼500 kA/m. Hence, extrapolation or other methods are needed in order to provide well-defined critical current density relations for finite element simulations.

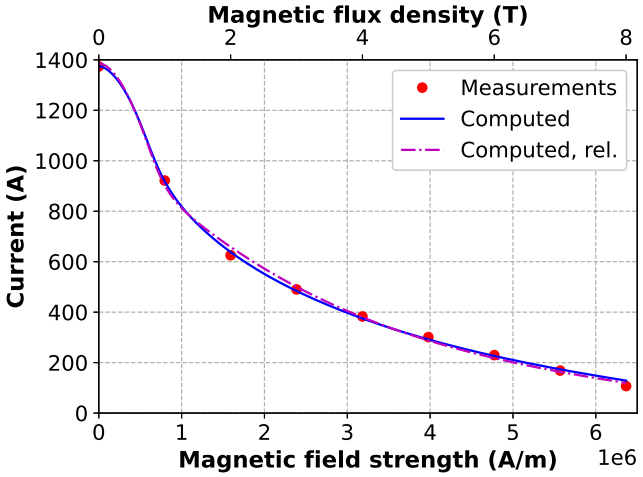

Fig. 4. Critical current measurements in 4.2 K according to Spencer *et al.* [6], and computed curves. The computational curves are obtained by applying the estimated critical current density relations in Fig. 3 to the forward model in Section III-A.

Using the estimated j_c, the critical current was computed and the results are depicted in Fig. 4. The curves 'Computed' and 'Computed, rel.' refer to the computational curves obtained by using the corresponding local critical current densities in Fig. 3 in the forward model. The error, given by (4), of the 'Computed' curve was 29.4 A, which is considered a reasonable fit. However, a good fit in the sense of (4) does not imply reliability of the estimated j_c. It may occur that portions of the estimated j_c are sensitive to measurement errors. Section V is dedicated to analyzing the sensitivity of the estimated j_c with respect to measurement errors. This gives the reader a more thorough access to assess the reliability of the results.

In Fig. 5, we see a field solution with a local current density and a magnetic self-field strength visualized. The wire in the figure is carrying a critical current of 129 A in an external magnetic field of 8 T. The solution corresponds to the rightmost 'Computed' point in Fig. 4.

The critical current of 129 A corresponds to a self-field roughly of the order of 50 kA/m on the boundary of the 0.81 mm wire. From Fig. 5, we conclude that the field solutions are in balance.

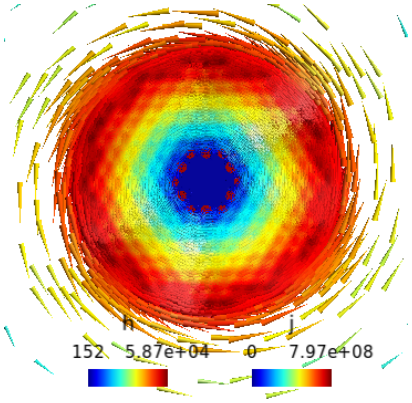

Fig. 5. This figure displays the local current density and the magnetic self-field strength in a situation where the wire is in critical state, carrying 129 A in an external field of 8 T. This situation corresponds to the rightmost 'Computed' point in Fig. 4.

IV. Remarks on Convergence

In the spirit of Rostila *et al.* [3], we briefly discuss the computational burden of the estimation process as well as the convergence of the minimization.

The FE discretized version of (1) in the geometry of Fig. 1 contains 5362 unknown nodal values for φ. The number of elements is 10860. Solving the I_c curve once requires solving 9 nonlinear static problems using the Newton's method, one for each measured magnetic field. To express the overall computational burden of the process, we repeated the estimation process once again but this time using the computational values $(h_{\text{meas},i}, I_c(h_{\text{meas},i}, \alpha))$, with α as in (5), as a 'measurement'. In principle, using these values in the estimation problem as 'measurements', the coefficients of the critical current density scaling relation should converge to α and the error e should converge to zero. Initial guess of $\alpha \approx [1,1,1,1] \cdot 10^9$ A/m^2 was chosen for the optimization algorithm. This guess is a reasonable but honest guess in the sense that it is of the correct order of magnitude but still relatively far from the estimated value of (5).

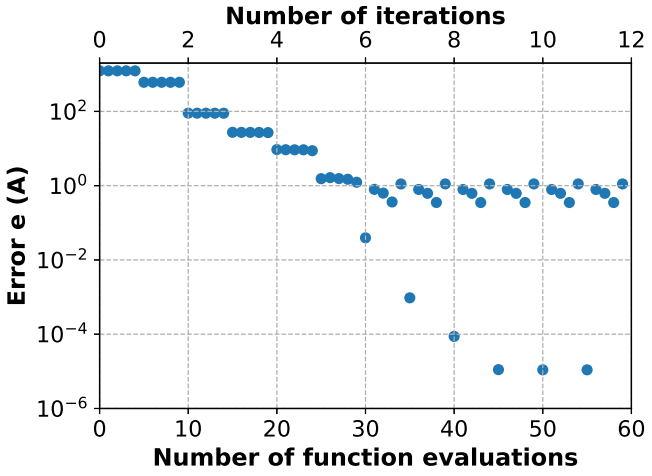

Fig. 6. Visualization of the convergence of the minimization of (4) in a practical situation. Each blue point represents one forward model evaluation.

In Fig. 6, we see the convergence of the method in terms of the error function (4) as a function of forward model evaluations. For a problem with a four dimensional unknown, five forward model evaluations are carried out per each iteration. It took 12 iterations, total 60 objective function evaluations, to achieve an error of $e \approx 3.7 \cdot 10^{-6}$ A/m^2. We conclude that the estimation method converges well with a reasonable computational burden.

V. Sensitivity to Measurement Errors

In the spirit of Rostila *et al.* [3], we analyze the sensitivity of the estimated j_c curve with respect to errors in the measured $I_{\text{c,meas}}$ values. In order to define measurement errors, we have to define 'exact' values of I_c where to compare the distorted values. We again define the computational values of $I_c(h_{\text{meas},i}, \alpha)$, with α as in (5), to be 'exact' and denote them by $I_{\text{exact},i}$. Of course, this is merely a definition.

A. Systematic measurement errors

We assume that the values $I_{\text{exact},i}$ are exposed to systematic errors. We used expressions of the form $(1+p)I_{\text{exact,i}}$ with

$$p = \pm 0.001, \pm 0.01, \pm 0.03, \pm 0.06, \pm 0.1$$

as measurements in the objective function (4). Then by using the Trust Region Reflective algorithm, we estimated the parameters α^p with p as an index denoting the chosen systematic error.

We choose the expression

$$\frac{\int_0^{h_{c2}} j_c(h,\alpha)dh - \int_0^{h_{c2}} j_c(h,\alpha^p)dh}{\int_0^{h_{c2}} j_c(h,\alpha)dh} \tag{8}$$

to denote the error between the 'exact' j_c and estimated ones. Since the expression of j_c (3) is very easy to integrate, we find an easy form of (8) given by

$$\frac{\sum_i \left(\frac{\alpha_i}{q_i+1}\right) - \sum_i \left(\frac{\alpha_i^p}{q_i+1}\right)}{\sum_i \left(\frac{\alpha_i}{q_i+1}\right)}, \tag{9}$$

where the numbers q_i denote the exponents defined in (3).

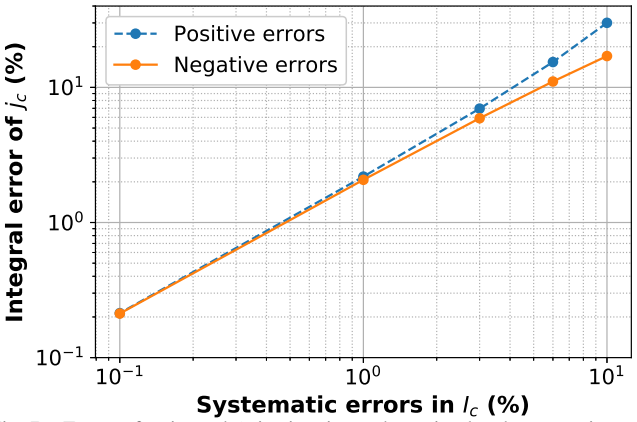

Fig. 7. Errors of estimated j_c in situations where simulated systematic errors of various orders are added to the measured I_c. The errors are quantified by the integral (8).

In Fig. 7, we see the errors in the estimated j_c, given by (9), with respect to the chosen systematic errors in I_c. The errors are depicted separately for positive and negative systematic errors. In the graph, we see that the integral error of j_c is of the same order as the systematic errors in measured I_c values but slightly higher.

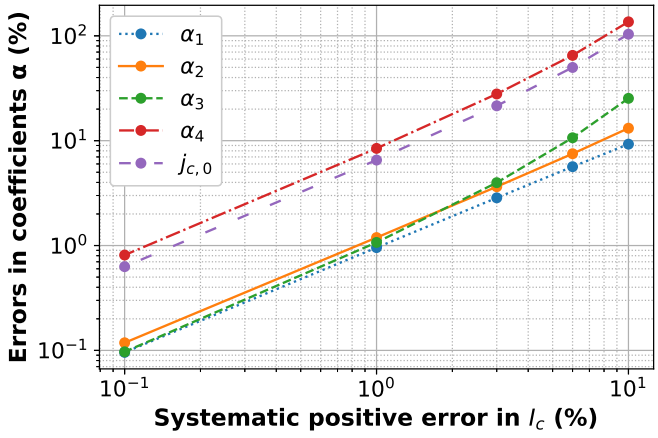

(a) Positive errors

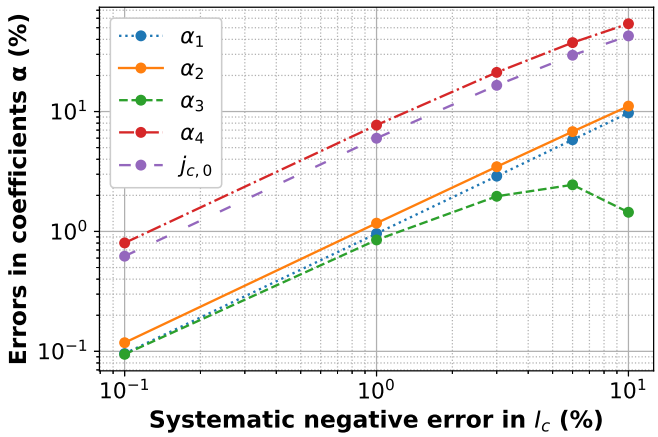

(b) Negative errors

Fig. 8. Errors of the estimated α-parameters in situations where simulated systematic errors of varoius orders are added to the measured I_c. Errors in the zero-field critical current density j_c are visualized as well.

Let us emphasize more the effect of systematic errors in I_c to the estimated parameters α of j_c. In Figs 8a and 8b, the individual errors of the estimated α-values are depicted for positive and negative measurement errors respectively. The errors of the α-values are defined by

$$\frac{\alpha - \alpha^p}{\alpha},$$

where α are the values of (5) and α^p are the estimated ones with the presence of simulated measurement errors. Both figures, 8a and 8b, have the same trend in general. For the values α_1^p, α_2^p and α_3^p, it seems that one percent of error in the measured I_c leads to one percent of error. However, the value α_4^p is more sensitive to measurement errors. One percent of measurement error in this case leads to 7-9% errors.

This α_4^p is the coefficient of the term in (3) with the highest exponent. In Figs 8a and 8b, we see that the error of α_4 is closely related to the error of the zero-field critical current density $j_{c,0} = \sum_i \alpha_i$, which is also quite sensitive to measurement errors.

We conclude that the integral error (8) gives relative errors of j_c of the same order as the relative errors of measured I_c. However, the curve j_c can be more sensitive to errors, especially in the range of very low external magnetic fields.

B. Random measurement errors

In the spirit of Rostila *et al.* [3], let us now consider random measurement errors. In the previous section, the 'exact' values of $I_{\text{exact},i}$ were altered in a systematic fashion, but this time we simulate random errors. Consider randomized numbers $r_{i,j}$ with index $j = 1, ..., 100$ and the index i corresponding to the index of $I_{\text{exact},i}$. The numbers $r_{i,j}$ are taken from a uniform distribution of $[-0.1, 0.1]$, $[-1, 1]$, $[-4, 4]$, $[-10, 10]$ or $[-40, 40]$ to define error tolerances. We set $I_{\text{j, i}} = I_{\text{exact},i} + r_{i,j}$. This means that the 'exact' values of I_c are altered randomly by adding uniformly distributed random components to each value. Minimizations of the objective function e, with $I_{\text{j, i}}$ as measurement data, were carried out for each of the five sets of one hundred randomized collections of data. The integral errors of (8) were computed and maximum values were chosen from both negative and positive errors. In Fig. 9, the maximum values of the integral error (8) are depicted.

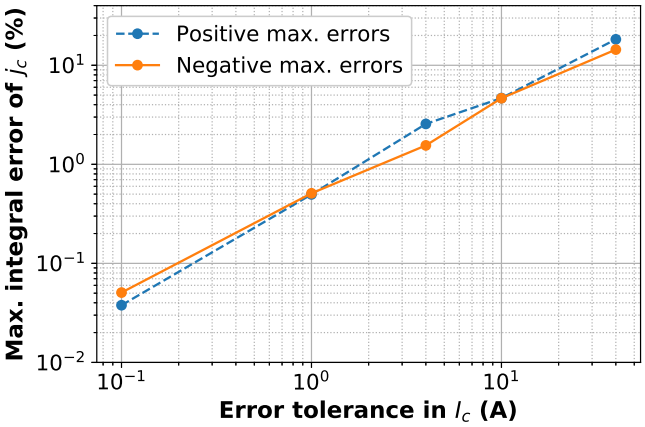

Fig. 9. Visualization of the positive and negative maxima of the integral errors (8) of j_c in situations where simulated randomized errors are added to I_c. The sample size of each simulation was 100.

Before we make any conclusions, let us consider the sensitivities of individual α-values. For each set of one hundred samples of the five error tolerances, we may take the maximum errors of the estimated α-values both for positive and negative errors comparing to the 'exact' values given by (5). The maximum positive and negative errors are depicted in Figs 10a and 10b, respectively.

It seems that the order of uncertainty of the integral error of j_c and the order of uncertainty of α_1 and α_2 more or less agree. The order of the uncertainties of α_3, α_4 and $j_{c,0}$, however, are notably larger. Again, the coefficients α_3 and α_4 correspond to the higher exponent terms in (3). Take for

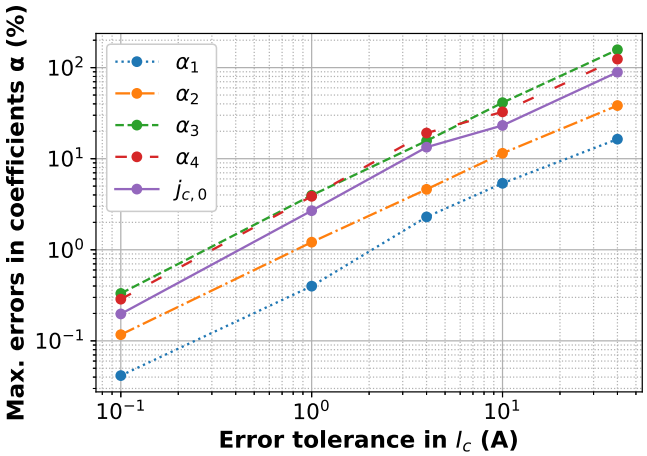

(a) Maximum positive errors

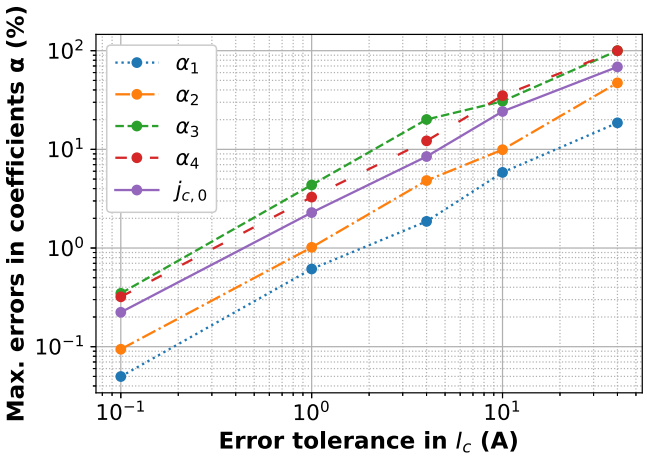

(b) Maximum negative errors

Fig. 10. Visualization of the maximum errors of the estimated α-parameters in situations where simulated randomized errors are added to I_c.

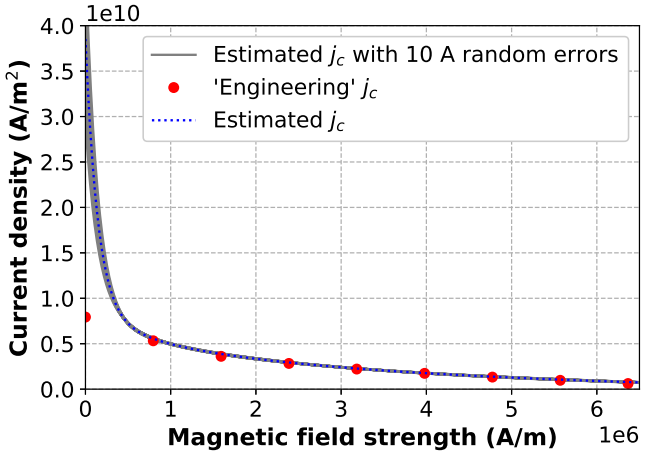

(a) With max. 10 A random errors added to I_c measurements

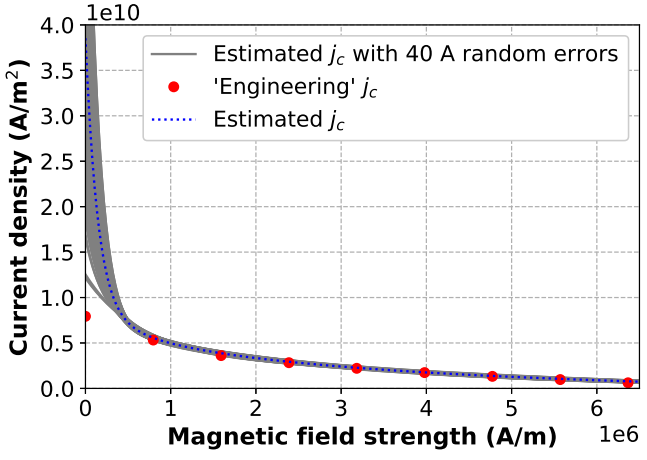

(b) With max. 40 A random errors added to I_c measurements

Fig. 11. Visualizations of the estimated j_c curves in situations where randomized errors are added to the measured I_c-values.

instance the highest error tolerance of 40 A in I_c. The integral error of j_c yields less than 20% of error in j_c, whereas the estimated zero-field critical current density $j_{c,0}$ has uncertainty of the order 90%. We conclude that also in the case of random errors, the uncertainty of the low-field critical current density is significantly higher than the uncertainty of the integral error of j_c.

To visualize the uncertainties further, in Figs 11a and 11b are depicted all of the estimated j_c curves with two error tolerances in simulated I_c measurements: 10 A and 40 A, respectively. In the figures, we can see that most of the uncertainties in the estimated j_c curves can be found in the low-field region below ∼500 kA/m. We note that even though the maximum errors in the individual α-values, depicted in Figs 10a and 10b, are relatively high, the shapes of the j_c curves in the high-field region above ∼500 kA/m are not greatly affected.

C. Rough estimate of random errors

To decide how uncertain the estimated j_c, given by the parameters α in (5) is, we assume that all the errors are due to random measurement errors. The final cost of the estimation problem was 29.4 A and the largest individual difference between measured and computed current was 21.6 A.

The first rough estimate for the uncertainty of the current measurements would be to assume that each of the nine current measurements is vulnerable to at least 9.8 A of random errors. This is due to the cost function (4) not being able to provide 29.4 A error if each nine measurements were within less than 9.8 A tolerance.

On the other hand, for each estimation of random errors in the previous section, we also computed the final costs e, defined by (4). Selecting the maximum and mean costs of each dataset, we find the cost vs. I_c error tolerance curves of Fig. 12. In the figure, there is also a line representing the final cost of the original estimation problem, 29.4 A. Only samples with error tolerance of I_c greater than ∼14 A provided final costs more than 29.4 A. Furthermore, the mean error reaches 29.4 A with error tolerances as high as ∼ 50 A.

These considerations suggest that the uncertainty of the estimated j_c should be found somewhere from the far right end of the Figs 9, 10a and 10b. In terms of maximum integral error of the estimated j_c, the uncertainty could be as high as

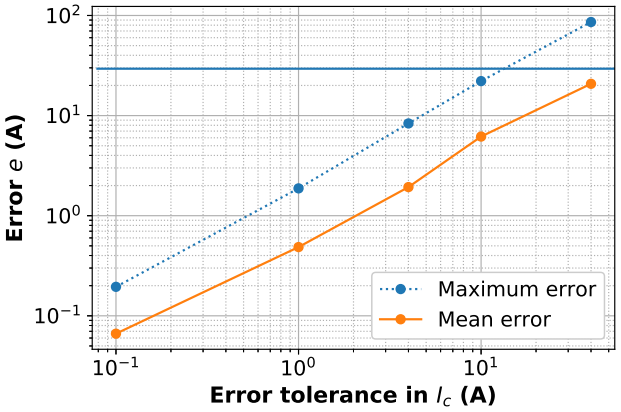

Fig. 12. The dependency between the error tolerances of the simulated random errors of I_c and the maximum and the mean values of the final costs (4) in forward simulations of critical current are visualized. As the cost function (4) yields a well-defined error, the tolerance of random errors in the measured I_c may be roughly estimated. The horizontal line corresponds to the error of 29.4 A of the original estimation.

some tens of percents. On the other hand, for the estimated zero-field critical current density, the uncertainty could be as high as a factor of two of the estimated value.

VI. Conclusion and Discussion

In this paper, the critical current density of NbTi was estimated from critical current measurements using a finite element method based estimation scheme. The method turned out to be of adequate computational burden. Even though the computational and measured critical currents may be matched accurately, sensitivity analysis of simulated systematic and random errors in current measurements revealed that the estimated zero-field critical current density, in particular, is very sensitive to critical current measurement errors.

As an extension, this study calls for the use of a more advanced forward model with the possibility to control the degree of twisting of the cable and the degree of couplings between the filaments in the presence of an externally applied magnetic field. The motivation is simple. If the self-field distribution in the wire is heavily affected by helicoidal shape of the filaments, the forward model is unable to capture such effects.

An approach for modeling twisted conductors in 2-D taking into account self-field effects has been reported [10], [11], [12]. The model exploits helicoidal symmetry. Straightforward generalization of the approach taking into account a uniform external magnetic field is not possible due to the requirements by the chosen symmetry, and the desired generalization remains as an open question. If self-fields suffice, this approach could very well be utilized for our purposes in the future.

Models with sliced 2-D geometries have been proposed, and in this case, both the twisting of the wire and externally applied fields may be included in the computations [17]. The degree of coupling between the filaments, however, is not an intrinsic property of the model.

An extension to 3-D taking into account external fields, twisting of the wire and the couplings between the filaments is also possible, of course with additional computational burden.

Acknowledgment

The foundation of Ulla Tuominen is acknowledged for financial support. J. Vesa acknowledges the discussions related to superconductivity in general, critical state and existing research on estimation problems with Janne Ruuskanen, Tiina Salmi and Antti Stenvall. Saara Göös is acknowledged for reading the manuscript and commenting on the style.

References

[1] L. Rostila, J. Lehtonen and R. Mikkonen, "Self-field reduces critical current density in thick YBCO layers", *Physica C*, vol. 451, no. 1, pp. 66-70, Jan. 2007.

[2] M. Garber, A.K. Gosh and W.B. Sampson, "The Effect of Self Field on the Critical Current Determination of Multifilamentary Superconductors", *IEEE Transactions on Magnetics*, vol. 25, no. 2, pp. 1940-1944, Mar. 1989.

[3] L. Rostila, J. Lehtonen, M. Masti and R. Mikkonen, "How to determine critical current density in YBCO tapes from voltage-current measurements at low magnetic fields", *Superconductor Science and Technology*, vol. 20, no. 12, pp. 1097-1100, Dec. 2007.

[4] F. Grilli, F. Sirois, V. M. R. Zermeño and M. Vojenčiak "Self-Consistent Modeling of the Ic of HTS Devices: How Accurate do Models Really Need to Be?", *IEEE Transactions on Applied Superconductivity*, vol. 24, no. 6, pp. 1-8, Dec. 2014.

[5] V. M. R. Zermeño, K. Habelok, M. Stepień and F. Grilli, "A parameter-free method to extract the superconductor's Jc(B,θ) field-dependence from in-field current–voltage characteristics of high temperature superconductor tapes", *Superconductor Science and Technology*, vol. 30, no. 3, Jan. 2007, Art. no. 034001.

[6] C.R. Spencer, P.A. Sanger and M. Young, "The Temperature and Magnetic Field Dependence of Superconducting Critical Current Densities of Multifilamentary Nb3Sn and NbTi Composite Wires", *IEEE Transactions on Magnetics*, vol. 15, no. 1, pp. 76-79, Jan. 1979.

[7] V. Zermeño, F. Sirois, M. Takayashu, M. Vojenčiak, A. Kario and F. Grilli, "A self-consistent model for estimating the critical current of superconducting devices", *Superconductor Science and Technology*, vol. 28, no. 8, Jun. 2015, Art. no. 085004.

[8] M. Spivak, *Calculus on Manifolds - A Modern Approach to Classical Theorems of Advanced Calculus*, W. A. Benjamin, Inc. New York, Amsterdam, 1965.

[9] G.A. Deschamps, "Electromagnetics and Differential Forms", *Proceedings of the IEEE*, vol. 69, no. 6, pp. 676-697, Jun. 1981.

[10] A. Stenvall, T. Tarhassaari, F. Grilli, P. Raumonen, M. Vojenčiak and M. Pellikka, "Manifolds in electromagnetism and superconductor modelling: Using their properties to model critical current of twisted conductors in self-field with 2-D model", *Cryogenics*, vol. 53, pp. 135-141, Jan. 2013.

[11] A. Stenvall, M. Siahrang, F. Grilli, and F. Sirois, "Computation of self-field hysteresis losses in conductors with helicoidal structure using a 2D finite element method", *Superconductor Science and Technology*, vol. 26, no. 4, Apr. 2013, Art. no. 045011.

[12] A. Stenvall, F. Grilli and M. Lyly, "Current-Penetration Patterns in Twisted Superconductors in Self-Field", *IEEE Transactions on Applied Superconductivity*, vol. 23, no. 3, Jun. 2013, Art. no. 8200105.

[13] J. Vesa and P. Rasilo, "Producing 3-D Imitations of Soft Magnetic Composite Material Geometries", *IEEE Transactions on Magnetics*, vol. 55, no. 10, pp. 1-10, Oct. 2019.

[14] L. Bottura, "A Practical Fit for the Critical SurEace of NbTi", *IEEE Transactions on Applied Superconductivity*, vol. 10, no. 1, pp. 1054-1057, March 2000.

[15] L. Bottura, "$J_C(B;T;\varepsilon)$ Parameterization for the ITER Nb3Sn Production", *IEEE Transactions on Applied Superconductivity*, vol. 19, no. 3, pp. 1521-1524, Jun. 2009.

[16] Scipy scipy.optimize.least_squares documentation, Cited in Apr. 2020, https://docs.scipy.org/doc/scipy/reference/generated/scipy.optimize.least_squares.html#scipy.optimize.least_squares.

[17] V. Lahtinen and A. Stenvall, "Toward Two-Dimensional Simulations of Hysteresis Losses in Partially Coupled Superconducting Wires", *IEEE Transactions on Applied Superconductivity*, vol. 24, no. 3, Sep. 2013, Art. no. 8200205.